

Permeation of Internal and External Monovalent Cations through the Catfish Cone Photoreceptor cGMP-gated Channel

LAWRENCE W. HAYNES

From the Department of Medical Physiology, the Neuroscience Research Group and Lions' Sight Centre, University of Calgary, Calgary, Alberta, T2N 4N1, Canada

ABSTRACT The permeation of monovalent cations through the cGMP-gated channel of catfish cone outer segments was examined by measuring permeability and conductance ratios under biionic conditions. For monovalent cations presented on the cytoplasmic side of the channel, the permeability ratios with respect to extracellular Na followed the sequence $\text{NH}_4 > \text{K} > \text{Li} > \text{Rb} = \text{Na} > \text{Cs}$ while the conductance ratios at +50 mV followed the sequence $\text{Na} \approx \text{NH}_4 > \text{K} > \text{Rb} > \text{Li} = \text{Cs}$. These patterns are broadly similar to the amphibian rod channel. The symmetry of the channel was tested by presenting the test ion on the extracellular side and using Na as the common reference ion on the cytoplasmic side. Under these biionic conditions, the permeability ratios with respect to Na at the intracellular side followed the sequence $\text{NH}_4 > \text{Li} > \text{K} > \text{Na} > \text{Rb} > \text{Cs}$ while the conductance ratios at +50 mV followed the sequence $\text{NH}_4 > \text{K} \approx \text{Na} > \text{Rb} > \text{Li} > \text{Cs}$. Thus, the channel is asymmetric with respect to external and internal cations. Under symmetrical 120 mM ionic conditions, the single-channel conductance at +50 mV ranged from 58 pS in NH_4 to 15 pS for Cs and was in the order $\text{NH}_4 > \text{Na} > \text{K} > \text{Rb} > \text{Cs}$. Unexpectedly, the single-channel current-voltage relation showed sufficient outward rectification to account for the rectification observed in multichannel patches without invoking voltage dependence in gating. The concentration dependence of the reversal potential for K showed that chloride was impermeant. Anomalous mole fraction behavior was not observed, nor, over a limited concentration range, were multiple dissociation constants. An Eyring rate theory model with a single binding site was sufficient to explain these observations.

INTRODUCTION

The cGMP-gated channels of rod and cone outer segments are responsible for creating the change in transmembrane voltage that occurs in response to illumination of the photoreceptor. The channels of both rods (Fesenko, Kolesnikov, and Lyu-

Address correspondence to Dr. L. W. Haynes, Department of Medical Physiology, University of Calgary, 330 Hospital Drive NW, Calgary, AB, T2N 4N1, Canada.

barsky, 1985; Furman and Tanaka, 1990; Menini, 1990; Colamartino, Menini, and Torre, 1991; Zimmerman and Baylor, 1992) and cones (Haynes and Yau, 1985; Picones and Korenbrot, 1992; Haynes, 1995) are nonspecific cation channels that pass both monovalent and divalent cations. The rectification characteristic of each channel under physiological conditions (Fesenko, Kolesnikov, and Lyubarsky, 1985; Yau, Haynes, and Nakatani, 1986) is the result of voltage-dependent block by divalent cations (Yau and Haynes, 1986). In the absence of divalent cations (Yau and Haynes, 1986), the channels of both rods (Haynes et al., 1986; Zimmerman and Baylor, 1986) and cones (Haynes and Yau, 1990) are unblocked and the current-voltage relations for both channels lose most of their rectification. What residual rectification remains has been attributed to a very weak voltage dependence in the open probability of the channel (Karpen, Zimmerman, Stryer, and Baylor, 1988*a,b*; Haynes and Yau, 1990).

Several investigators have made use of Eyring rate theory to model the permeation process through either the rod (Zimmerman and Baylor, 1992) or cone (Picones and Korenbrot, 1992) channels. These studies have generally used sodium as the extracellular reference ion and have varied the intracellular ion. This kind of experiment provides information mostly about the intracellular side of the energy profile. Ideally, identical experiments would be performed changing the ions on the extracellular side of the channel, but this cannot be done for several reasons. First, it has not been possible to obtain outside-out patches from photoreceptors because the disks tightly anchored to the plasma membrane seem to preclude re-sealing of the patch in the outside-out configuration. Second, bilayer studies are not possible for the cone channel because there is no method to either purify the cone channel from rod channels or the cone outer segments from rod outer segments. Third, it has not been possible to vary the ion inside the pipette in a quantitative way, precluding truly biionic experiments. This has forced the assumption that the channel is symmetric, i.e., that the heights of the barriers and the depths of the wells are the same for intracellular and extracellular ions.

The two different approaches have been taken in this study. In the first set of experiments, I have determined the permeability and conductance ratios for a variety of monovalent cations presented on the cytoplasmic side of the patch with sodium as the reference ion at the extracellular side. In the second set of experiments, I began with the test ion bathing both sides of the channel and then always switched to sodium on the cytoplasmic side of the channel as the reference ion. The results were then compared with those obtained using the first method to determine if any asymmetry of the permeation pathway existed. In addition, experiments measuring the concentration dependence of conductance and reversal potential provided information about the strength of the binding site(s), their number and anion permeability. Multiple occupancy of the channel was tested by looking for anomalous mole fraction effects. Recordings from single-channel patches were used to determine if the rectification present in current-voltage relations obtained from multi-channel patches was the result of the permeation process or voltage dependence in the gating process. These results were incorporated into a single site Eyring model.

This work has previously been described briefly in abstract form (Haynes, 1991, 1993, 1994).

METHODS

Preparation

Recordings were made from excised, inside-out patches of plasma membrane obtained from the tip of a cone outer segment of the channel catfish, *Ictalurus punctatus*. Each fish was dark adapted and then killed by decapitation. The retinas were dissected out and enzymatically cleaned using 0.5 mg ml⁻¹ hyaluronidase (type IV, Sigma Chemical Co., St. Louis, MO) and 0.05 mg ml⁻¹ collagenase (type IV; Sigma Chemical Co.) for a total of 30 min. Pieces of retina were stored in ice-cold Ringer's solution consisting of (in millimolar): 110 NaCl, 2.5 KCl, 1.6 MgCl₂, 1.0 CaCl₂, 5.0 Glucose, and 5.0 Na HEPES (pH 7.6) until needed. A small slip of razor blade was used to triturate the retina, yielding a dispersion of isolated cells and broken outer segments which were collected, transferred to the experimental chamber and allowed to settle. Cells that did not settle, and any residual traces of Ringer's solution, were washed from the chamber by the saline solution before the first patch pipette was introduced. Cells were replaced frequently during the course of a day's experiments.

Solutions

The pipette and bath solutions were initially identical in each experiment. With the ions symmetrically distributed across the patch of plasma membrane, the driving force for current flow came only from the holding potential. Channel activity was elicited by substituting a second bath solution containing the sodium salt (in sodium-containing solutions) or the free acid (in sodium-free solutions) of guanosine 3', 5' cyclic monophosphate (cGMP, Sigma Chemical Co.). In the case of single-channel recordings, a low concentration (1–10 μM) of cGMP was used to activate only a few of the channels in the patch. In the case of ramped current-voltage relations, 1 mM cGMP was used to activate all of the channels in the patch fully. The bath solution could be changed rapidly ($\tau < 300$ ms) to expose the cytoplasmic surface of the patch to various bath solutions. All experiments were done at room temperature (22–24°C).

Each solution contained the chloride salt of a monovalent cation together with the monovalent cation salt of EGTA, EDTA, and HEPES at pH 7.6. In all cases, the concentrations of these minor constituents were (in millimolar) 0.1 EGTA, 0.1 EDTA, and 5.0 HEPES. In experiments where the concentration of the cation was reduced, mannitol was used to maintain tonicity since all organic cations tested (choline, tetramethyl-, tetraethyl- and tetrapropylammonium, *N*-methyl-D-glucamine and Tris) produced at least some block of the channel (Stotz and Haynes, 1995). The activity coefficients were calculated using the parametric equations of Pitzer and Mayorga (1973). Molarity and molality conversion was performed according to the formulas in Robinson and Stokes (1970). For convenience, all references to concentration in this paper are to the concentration of the solution as mixed. The actual ion activity is given in the text where appropriate.

Electrical Recordings

Patch pipettes were fabricated from thick-walled borosilicate glass (Corning 7740, A-M Systems, Everett, WA), coated with Sylgard 184 (Dow Corning Corp., Midland, MI) and fire polished. Normally, the pipette tip inside diameter was ~0.5 μm and resistances were typically 20–30 MΩ when filled with the saline solution described above. Pipettes pulled for experiments using internal perfusion of the pipette had somewhat larger tip diameters and resistances between 10 and 20 MΩ.

Current flowing across the patch was measured under voltage clamp by an Axopatch 1D patch clamp amplifier (Axon Instruments, Inc., Foster City, CA) with a bandwidth of DC to 20 kHz (–3 dB, 4-pole Bessel filter). The signal from the patch clamp was recorded on video tape using a PCM adapter. Patches were generally held at 0 mV, but in some cases (such as in Figs. 1 and 6) the stability of the patch could be enhanced by setting the holding potential to the reversal potential of

the leak. This potential, together with the junction potential (see below), was corrected for in plotting the current-voltage relations. It should be noted that the selectivities of the leak and the cGMP-gated channels under biionic conditions were not identical. Current-voltage relations were obtained under computer control by generating pairs of voltage ramps from the holding potential. In the first ramp, the voltage was stepped from the holding potential to the most negative potential (-60 or -80 mV) and then ramped at 120 mV s^{-1} to the most positive potential ($+60$ or $+80$ mV). In the second ramp, the process was repeated from the most positive to the most negative potential. The resulting currents were filtered at 250 Hz (-3 dB, 8-pole Bessel), digitized at $1,000$ Hz and stored on the computer's hard disk. Before subsequent analysis, the currents from the two ramps were averaged at each voltage to eliminate capacitive currents. In accordance with the standard physiological convention, currents flowing from the cytoplasmic side to the extracellular side are considered positive and positive potentials refer to positive voltages on the cytoplasmic side of the patch.

Data Analysis

Current-voltage relations were determined by averaging the digitized points during each voltage ramp, as described above. The leakage current was determined for each voltage by administering a pair of ramps before and after the application of cGMP. The average currents from each pair were in turn averaged together and subtracted from the average current in the presence of cGMP to obtain the net cGMP-dependent current. Only the net current is shown in the figures.

Liquid junction potentials were calculated using the activity of the ions involved (Barry and Lynch, 1991; Neher, 1992). Since the initial bath solution (before seal formation) and the pipette solution were identical, the only liquid junction potential in the system was between the various bath solutions and the 1 M KCl agar bridge connecting the bath to the ground electrode. Such potentials are small (<2 mV) and more accurately calculated than measured. The calculated liquid junction potential for each solution was used as a correction factor to shift the current-voltage relation along the voltage axis during plotting. Reversal potentials were determined by examination of such plots. Under biionic conditions (i.e., with only one permeant ion on each side of the membrane), the permeability ratio of ion X at the intracellular surface with respect to ion Y of the same valence at the extracellular surface can be obtained directly from the shift in the reversal potential using the biionic form of the Goldman-Hodgkin-Katz equation (e.g., Hille, 1992)

$$\frac{P_X}{P_Y} = \frac{[Y]_o}{[X]_i} e^{-\frac{zF\Delta V_{Rev}}{RT}} \quad (1)$$

where P_X/P_Y is the permeability ratio of ion X with respect to ion Y , ΔV_{Rev} is the change in reversal potential, the subscripts i and o refer to the cytoplasmic and extracellular surfaces of the patch, respectively, z is the valence of the ions and R , T , and F have their usual thermodynamic meaning. While most (if not all) ion channels violate the assumptions of the GHK equations (e.g., independence), this equation is nonetheless generally used to define the permeability ratio for the purposes of comparison with other channels. Conductances were measured at a fixed membrane potential, given in the text, to avoid any possible effects of voltage-dependent gating. All conductances were chord conductances, determined by dividing the current at a given voltage by the driving force. Because the macroscopic current depends on the number of channels present in the patch, it is essential that the patch neither gains nor loses channels during the course of the experiment. In patches with only a few channels, this was not always the case. Observation of single-channel patches (Haynes, unpublished observation) has shown that channels can be lost (or gained) during the course of an experiment, presumably by moving between the patch and the membrane-glass seal area. This was checked for whenever possible by repeating the current-volt-

age relation in symmetrical sodium solutions one or more times over the course of the experiment.

The single-channel conductance for different monovalent cations under symmetrical conditions was determined from the currents of individual channel openings obtained at a low concentration of cGMP (Haynes and Yau, 1990). For these recordings, the signal was low-pass filtered to 2.5 kHz (-3 dB, 8-pole Bessel) during playback and digitization. Continuous stretches of record were digitized at 20 kHz, stored on the computer's hard disk, and later analyzed by the IPROC2 program (Axon Instruments, Inc.). The arithmetic mean of the amplitudes of individual openings was computed by the program and taken as the single-channel current. This value was checked against the value obtained by fitting the open-event amplitude histogram with a single gaussian (e.g., Figs. 3 and 7). In all experiments of this kind, the solutions bathing both sides of the patch were identical and the driving force came only from the holding potential.

Throughout, data are presented as mean \pm SD. All statistical tests of the differences between means used the two-sided *t* test. The number of degrees of freedom in such tests is indicated throughout the text as *df*.

Eyring rate theory models were fitted to the data using a least-squares method. The portion of the program that generated the predicted currents used the algorithm described by Alvarez, Villarreal, and Eisenman (1992), implemented in C, and generalized to accommodate an arbitrary combination of sites and monovalent or polyvalent ion species. Surface charge effects were calculated using the Grahame equation (Grahame, 1947). The conventions and standard state used here are those described by Alvarez et al. (1992).

Eyring rate theory predicts the current for a single channel, but most data comes from patches with more than one channel. This macroscopic current is related to the single-channel current by (e.g., Hille, 1992)

$$I = NP_o i \quad (2)$$

where *i* is the single-channel current, *N* is the number of channels in the patch and *P_o* is the (possibly voltage-dependent) probability that the channel is open. Using Eq. 2, it is possible to correct the macroscopic current if one knows the single-channel current by scaling the macroscopic current by the factor *NP_o*. Estimates for the single-channel amplitude came from steady state recordings of individual channel openings elicited by a low concentration of cGMP at various voltages and from ramped current-voltage relations obtained from four patches each containing a single channel activated by a saturating concentration of cGMP (1 mM).

RESULTS

Permeability and Conductance of Intracellular Monovalent Cations

Permeability and conductance ratios were determined by measuring reversal potentials and conductances under biionic conditions, i.e., with only sodium as the permeant ion on the extracellular side of the membrane and the test ion as the permeant ion on the cytoplasmic side of the membrane. Under these conditions, a reversal potential positive to 0 mV indicates an ion with a lower permeability than sodium. Fig. 1 shows a typical example of such an experiment for a patch with ~22 channels. In all experiments of this type, the cation concentration was 120 mM, corresponding to activities (in millimolar) of 94 (Li), 92 (Na), 89 (K), 90 (Rb), 88 (Cs), and 90 (NH₄). It is clear from this experiment that most of the reversal potentials were tightly clustered at ~0 mV, indicating that the channel does not discriminate well among these ions. Ammonium was slightly more permeant than sodium

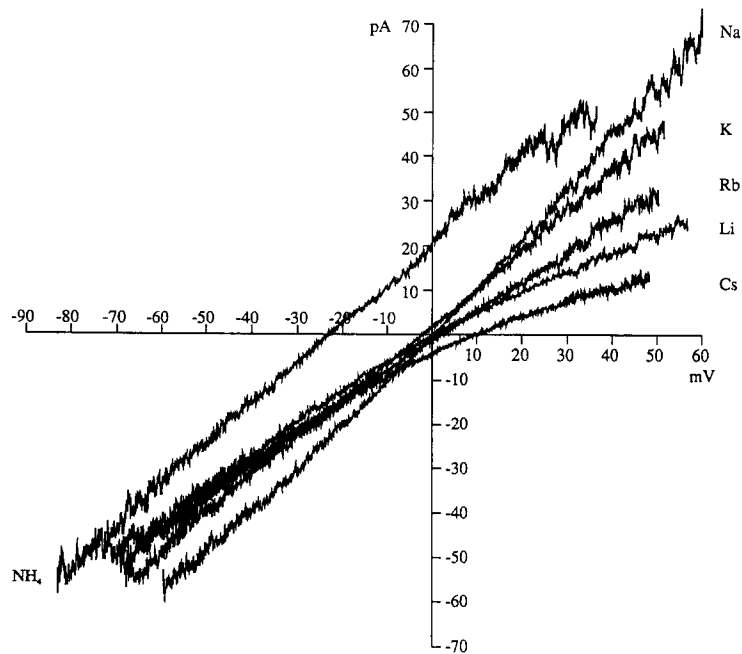


FIGURE 1. Current-voltage relations under 120 mM biionic conditions with Na as the extracellular ion. Li, Na, K, Rb, Cs, or NH_4 was present on the cytoplasmic side of the patch at an activity of 94, 92, 89, 90, 88, and 90 mM, respectively, and Na was present on the extracellular side with activity of 92 mM. The reversal potential for each of these ions was +0.4, 0, -2.2, +1.7, +9.7, -23.5 mV and the conductance ratio at +50 mV was 0.41, 1.0, 0.78, 0.56, and 0.30. The conductance ratio for NH_4 at +50 mV could not be determined in this experiment. All traces from a single patch.

and cesium was slightly less permeant, with the rest being nearly equal. Yet while several of these cations had marginally higher permeability ratios, none conducted current through the channel as well as sodium. The ions with the lowest conductance ratios were lithium and cesium, which had $\sim 40\%$ of the conductance of sodium.

The similarity of the reversal potentials necessitated a large number of experimental trials so that the permeability and conductance ratios could be determined as accurately as possible. These results are summarized in Table I. The average permeability ranged from 2.31 for NH_4 to 0.79 for Cs and conductance ratios ranged from 1 for Na to 0.38 for Cs. Overall, the permeability ratios ranked in the order of $\text{NH}_4 > \text{K} > \text{Li} > \text{Rb} = \text{Na} > \text{Cs}$, and the chord conductance ratios at +50 mV ranked in the order $\text{Na} \approx \text{NH}_4 > \text{K} > \text{Rb} > \text{Li} = \text{Cs}$. Within the experimental error, these results are identical to those of Picones and Korenbrot (1992) obtained from bass cones under 157 mM biionic conditions with the exception of ammonium, which they did not test.

TABLE I
Permeability and Conductance Ratios: 120 mM

Ion	Intracellular			Extracellular			Symmetric		
	P_x/P_{Na}	n	G_x/G_{Na}	n	P_x/P_{Na}	n	G_x/G_{Na}	n	γ (pS)
Li	$1.10 \pm 0.10^*$	12	$0.39 \pm 0.13^*$	10	$1.16 \pm 0.15^*$	9	$0.66 \pm 0.09^{*\ddagger}$	9	ND
Na	1.0	22	1.0	22	1.0		1.0		48
K	$1.19 \pm 0.08^*$	9	$0.83 \pm 0.18^*$	7	$1.05 \pm 0.04^{*\ddagger}$	6	$1.09 \pm 0.13^\ddagger$	6	45
Rb	1.01 ± 0.09	8	$0.63 \pm 0.09^*$	8	$0.94 \pm 0.05^{*\ddagger}$	12	$0.82 \pm 0.11^{*\ddagger}$	12	25
Cs	$0.79 \pm 0.09^*$	7	$0.38 \pm 0.09^*$	7	$0.78 \pm 0.10^*$	13	$0.46 \pm 0.09^*$	13	15
NH ₄	$2.31 \pm 0.25^*$	8	0.89 ± 0.29	7	$2.29 \pm 0.29^*$	5	$2.32 \pm 0.88^{*\ddagger}$	5	58

All values given as mean \pm SD for the given number (n) of experiments. Conductances measured at +50 mV. γ = single-channel conductance under 120 mM symmetric conditions at +50 mV. ND = not determined. *Significantly different from Na at $p < 0.05$ (comparison made between data in the same column). \ddagger Significantly different from intracellular value at $p < 0.05$ (comparison made between data in the same row).

Permeability and Conductance Ratios for Extracellular Ions

The current-voltage relations obtained from five different patches under biionic conditions reversed from those just described, i.e., with Na on the intracellular side of the channel as the common reference ion, are shown in Fig. 2. For each patch, the experiment began with 120 mM NH₄, Li, K, Rb, or Cs bathing both sides of the membrane (activities the same as above). Under this symmetrical condition, the reversal potential was always 0 mV. The solution bathing the cytoplasmic side of the patch was then replaced with one containing 120 mM Na and the shift in the rever-

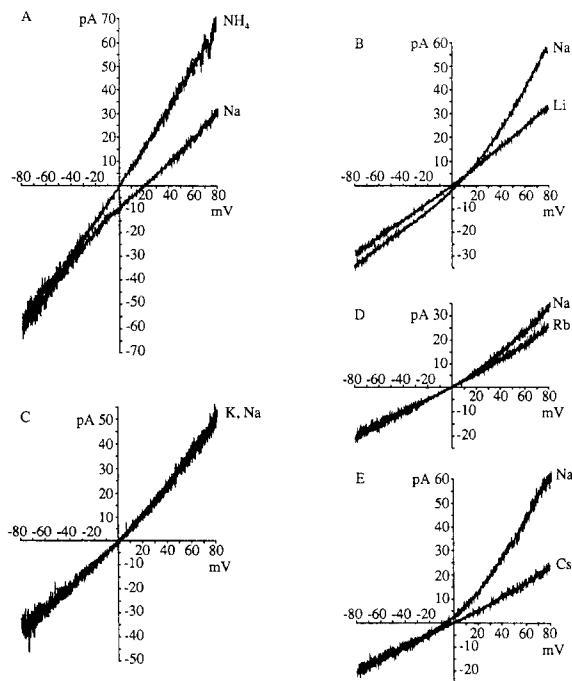


FIGURE 2. Current-voltage relations under 120 mM biionic conditions with Na as the intracellular ion. Current-voltage relations were obtained with 120 mM NH₄ (A), Li (B), K (C), Rb (D), or Cs (E) as the extracellular ions and Na as the intracellular ion (activities same as in Fig. 1). All experiments are from different patches. In all cases, the test ion was initially present on both sides of the channel, then Na was substituted on the cytoplasmic side of the channel. The reversal potential for each experiment was +20, +3.75, +1.75, 0, and -6.5 mV, respectively. The conductance ratios at +50 mV for each experiment were 1.7, 0.6, 0.96, 0.75, and 0.45, respectively.

sal potential was measured. Under these conditions, a reversal potential positive to 0 indicates a permeability ratio >1 for the test ion relative to Na. As was the case for the previous set of experiments, none of the ions showed a large shift in the reversal potential, with the largest shift in Fig. 2 being +20 mV for NH_4 . The mean permeability ratios, and the number of experiments for each ion, are given in Table I. With the exception of NH_4 , all of the permeability ratios were close to 1, as expected for a nonspecific cation channel. Ranked in descending order, the average permeability ratios formed the sequence $\text{NH}_4 > \text{Li} > \text{K} > \text{Na} > \text{Rb} > \text{Cs}$. Thus, the channel has slightly lower ratios for extracellular K and Rb compared with the values found for these ions on the intracellular side of the channel. These differences, while small, are statistically significant.

The current-voltage relations in Fig. 2 also show that Li, Rb, and Cs supported less current than sodium at positive potentials, while the current supported by K equalled that of Na. Only NH_4 supported more current than Na. The average conductance ratios for the currents at +50 mV ranged from 0.46 for Cs up to 2.3 for NH_4 (see Table I), and were in the order $\text{NH}_4 > \text{K} = \text{Na} > \text{Rb} > \text{Li} > \text{Cs}$. Note that, as in the previous set of experiments, these are measurements of outward current and are therefore not a measure of the relative ability of the various ions to cross from the extracellular to the intracellular side of the channel. Instead, the conductance ratios reflect the ability of Na compete against the other ions. It would seem that intracellular sodium is not as good as extracellular sodium at occupying the channel and carrying current.

Single-Channel Conductance under Symmetrical Conditions

Single-channel currents were measured for each of the ions (except Li) under symmetric ionic conditions (120 mM of the ion on both sides of the patch, activities as above) so that the current-voltage relations obtained from multichannel patches like those in Fig. 2 could be scaled for use in the Eyring rate theory modeling. Single-channel currents could not be obtained in Li because their small size (<1 pA) coupled with destabilization of the seal by Li made reliable analysis impossible. Sample currents obtained at +50 mV from five different patches are shown in Fig. 3 A. The size of the currents in these experiments paralleled the conductance ratios observed before; NH_4 supported the largest currents followed by Na, K, Rb, and Cs with the smallest currents. The single-channel conductance at +50 mV for each of these ions was 58, 48, 45, 25, and 15 pS, respectively.

The rectification seen in current-voltage relations obtained from patches containing more than one channel, as was the case for the majority of the experiments presented here, can come about from either the voltage dependence of the gating process or from the intrinsic rectification of the permeation process. Voltage dependence in the gating of the rod channel is known to occur (Karpen et al., 1988*a,b*). Likewise, previous measurements of single-channel openings recorded from multichannel cone patches over a limited range of voltages suggested that the current-voltage relation of the open channel was linear (Haynes and Yau, 1990), which implied that the rectification of the current-voltage relation of the cone channel was also due to voltage dependence in the gating. The results from experiments like those in Fig. 3 suggest that the single-channel current-voltage relation is

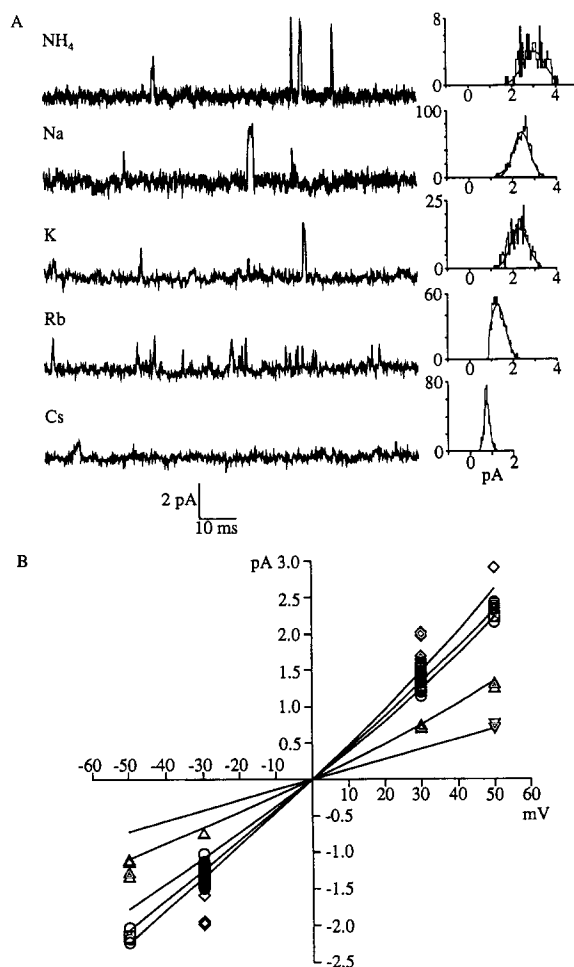


FIGURE 3. Single-channel conductances under 120 mM symmetric conditions for NH₄, Na, K, Rb, and Cs. (A) Sample traces obtained at +50 mV with a bandwidth of 2.5 kHz. 120 mM of the indicated ion bathed both sides of the patch. Each trace is from a different patch. The size of the single-channel current was greatest in NH₄ and smallest in Cs. The inset with each trace shows the open-amplitude histogram obtained from analysis of the full stretch of data from which the sample was excerpted. Each histogram is fitted with a single gaussian curve with a mean \pm SD for NH₄, Na, K, Rb, and Cs (respectively) of 3.01 ± 0.51 , 2.42 ± 0.37 , 2.31 ± 0.39 , 1.29 ± 0.31 , and 0.76 ± 0.13 pA. (B) Current-voltage relations for the single-channel currents under symmetric ionic conditions for NH₄ (\diamond , $n = 11$), Na (\circ , $n = 80$), K (\square , $n = 6$), Rb (\triangle , $n = 11$) and Cs (∇ , $n = 3$, data at +50 mV only). The lines are the current-voltage relations predicted by the single-site Eyring rate theory model shown in Fig. 8 (parameters in Table II). From top to bottom at +50 mV, the traces are in the order NH₄, K, Na, Rb, Cs.

outwardly rectifying, rather than linear. Therefore, at least part of the rectification of the macroscopic current must be due to permeation. To test this interpretation, experiments were conducted in which current-voltage relations were obtained over a wider voltage range from patches containing only a single channel. The current-voltage relation from a patch containing a single channel bathed in symmetric 120 mM sodium solutions and activated by 1 mM cGMP is shown in Fig. 4. Because the current in this experiment is nonstationary and because the open probability is in any case too high for analysis in the usual fashion, amplitude histograms could not be obtained. A patch was judged to contain a single channel if the current at, say, +50 mV matched that expected from a single channel (compare Figs. 3 B and 4) and if only a single open level was observed during the brief period in which cGMP was washed onto or off of the patch (i.e., no stacking of events was observed).

The current-voltage relation in Fig. 4 shows a slight outward rectification. Three other patches containing a single channel were obtained and all showed similar outward rectification. Because there is only a single channel in the patch, there can be no effect on the current of changing the open probability unless the open and closed durations are much shorter than the time constant of the low-pass filter used to condition the data, resulting in averaging together the open and closed current levels. This possibility was checked by increasing the filter cut-off frequency by eightfold from 250 Hz to 20 kHz (corresponding to changing the filter's "dead time" [Colquhoun and Sigworth, 1983] from ~ 720 to ~ 9 μ s). While the current noise increased substantially, the shape of the current-voltage relation was unchanged (data not shown). It seems unlikely, therefore, that the rectification seen in current-voltage relations of single-channel patches is due to filtration, although this remains a possibility given the rapid gating kinetics of the cGMP-gated channels (Haynes and Yau, 1990; Torre, Straforini, Sesti, and Lamb, 1992; Picones and Korenbrot, 1994). It is also unlikely that this rectification is due to block by residual divalent cations, because the shape of the current-voltage relation in the presence of divalent cations is very different.

The macroscopic currents obtained from the multichannel patches could be scaled to match the currents obtained from the single-channel patches by simply dividing the macroscopic current by a constant (voltage-independent) value representing the number of channels in the patch. All of the rectification of the macroscopic current-voltage relation can, therefore, be accounted for by the rectification present in the current-voltage relation of a single cone channel without invoking a voltage-dependent change in the open probability of the channel.

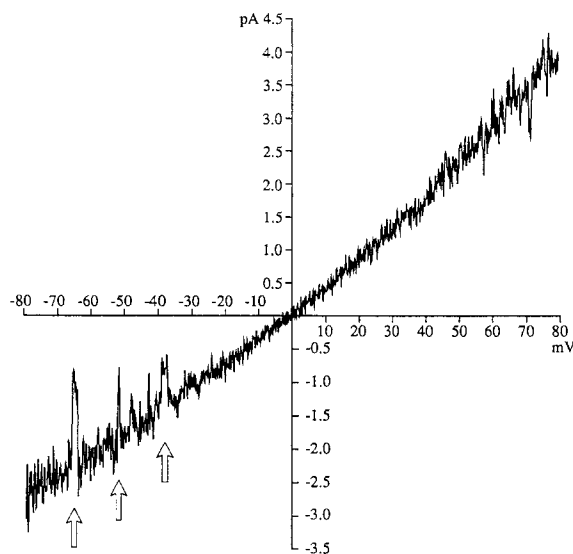


FIGURE 4. Current-voltage relation from a patch containing a single channel. The patch was bathed in symmetrical 120 mM Na solutions (92 mM activity). The slight outward rectification seen in this patch and the three other single-channel patches was present regardless of the cut-off frequency of the filter up to the highest value tested (20 kHz). Note that the channel closures indicated by the arrows reach no more than halfway to zero because two sweeps are averaged to produce the plotted trace, and the closures occurred in only one of the two sweeps. Based on a measured single-channel conductance of 48 pS (at +50 mV), the expected current at +50 mV is 2.4 pA, in good agreement with the 2.3 pA observed.

Lithium Vs Sodium Mole Fraction Behavior

One indication that a channel can be occupied by more than one ion at a time is the presence of an anomalous mole fraction effect in the conductance of the channel. In a multiple occupancy channel, the conductance depends on the relative occupancy of the channel by the two ions and the magnitude of the ion-ion interactions within the channel. An anomaly would be visible as a decrease, followed by an increase in conductance as the mole fraction (and therefore, the channel occu-

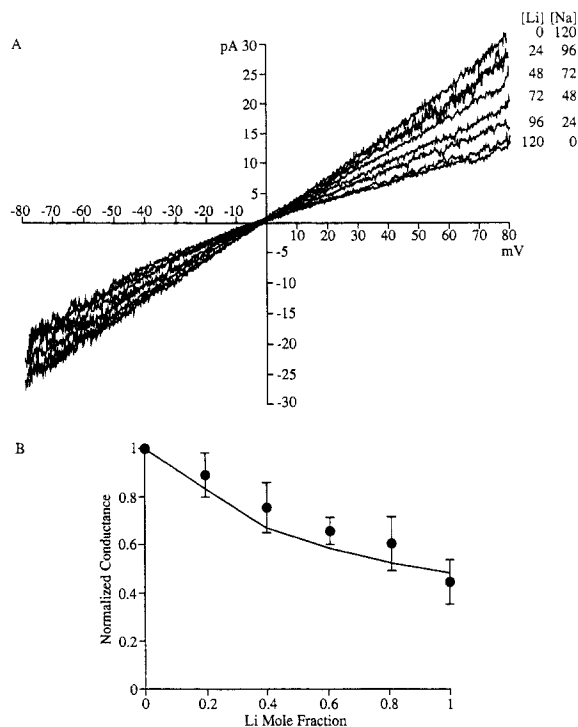


FIGURE 5. Lithium/sodium mixtures did not show anomalous mole fraction behavior. Lithium and sodium were mixed at constant total molarity to yield a lithium mole fraction of 0, 0.2, 0.4, 0.6, 0.8, or 1. (A) Current-voltage relation. There are two traces each for 0 Li, 120 Na, and for 120 Li, 0 Na and one trace for each of the other concentrations. (B) Plot of the normalized conductance at +50 mV as a function of the lithium mole fraction ($[\text{Li}] / ([\text{Na}] + [\text{Li}])$), at the cytoplasmic side of the patch. The chord conductance at +50 mV is normalized to that obtained in 100% sodium (96 mM activity, no lithium). The filled circles show the mean value from eight determinations in seven different patches whereas the error bars show the standard deviation. The line is that predicted by the single-site Eyring rate theory model shown in Fig. 8 (parameters in Table II). The conductance decreased monotonically as a function of the mole fraction.

pancy) changed. Lithium was chosen as the test ion for this experiment for two reasons. First, its conductance has the largest difference from that of sodium, suggesting that it binds more tightly within the channel than does sodium. One might expect to see an anomaly in the mole fraction behavior of the ion with the tightest binding to the channel since this would give the greatest opportunity for ion-ion interaction to alter the binding strength. Second, its permeability ratio is close to sodium which should minimize any shift in reversal potential. An example of such an experiment is shown in Fig. 5 A. The conductance decreased monotonically as

the mole fraction of lithium was increased. In none of the eight experiments summarized in Fig. 5 *B* was there any indication of an anomaly in the mole fraction behavior.

Concentration Dependence of the Reversal Potential

Because the cone channel displayed remarkably little selectivity with respect to monovalent cations, it was of interest to determine how selective it was for cations over anions. This was determined by examining the relation between the reversal potential and ion concentration over a wide range of concentration ratios. Cur-

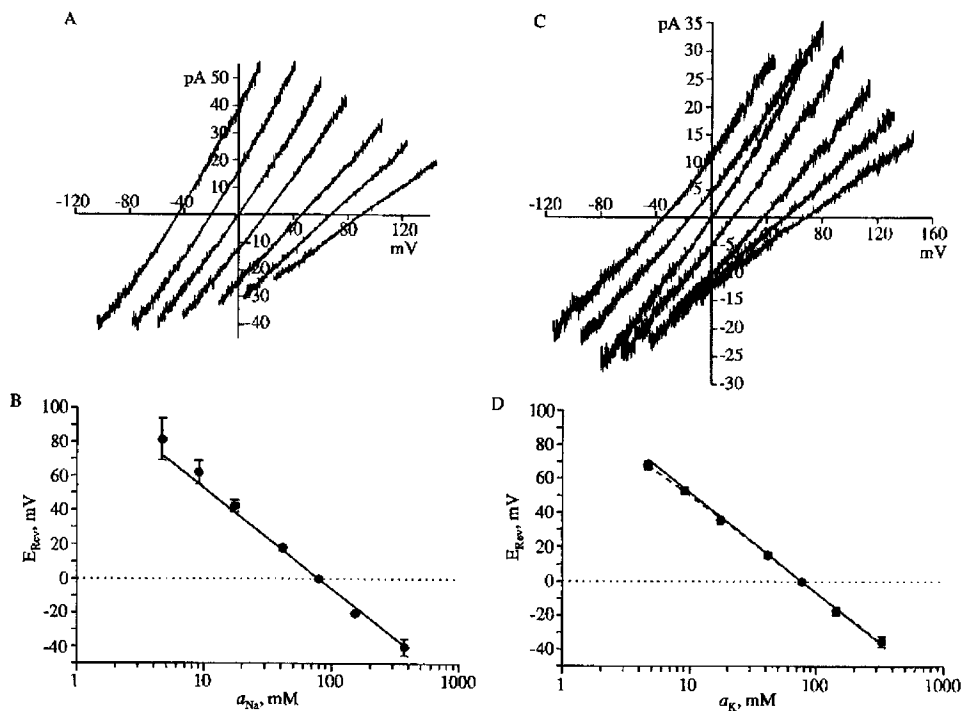


FIGURE 6. Dependence of the reversal potential on concentration. (A) Current-voltage relations obtained with 100 mM Na present on the extracellular side of the patch and 500, 200, 100, 50, 20, 10, or 5 mM Na present on the cytoplasmic side. The activities were 374, 152, 79, 41, 17, 9, and 5 mM, respectively. The reversal potentials were -40.9 , -19.8 , 0 , $+17.9$, $+44.4$, $+65.4$, and $+87.4$ mV. (B) Reversal potential as a function of Na activity. The circles show the mean reversal potential at each concentration for nine experiments and the error bars show standard deviations. The solid line is the prediction of the Nernst equation. The dotted line indicates 0 mV. (C) Current-voltage relations obtained with 100 mM K present on the extracellular side of the patch and 500, 200, 100, 50, 20, 10, or 5 mM K present on the cytoplasmic side. The activities were 329, 144, 77, 41, 17, 9, and 5 mM, respectively. The reversal potentials were -34.3 , -14.7 , 0 , $+15.7$, $+38.3$, $+53.9$, and $+68.6$ mV. (D) Reversal potential as a function of K activity. The circles show the mean reversal potential at each concentration for nine experiments and the error bars show standard deviations. The solid line is derived from the Nernst equation. The dashed line is derived from the GHK equation with a $P_{\text{Cl}}/P_{\text{Na}}$ ratio of 0.009. The dotted line indicates 0 mV.

rents were measured with 100 mM sodium in the pipette and 500, 200, 100, 50, 20, 10, or 5 mM sodium (activities of 374, 152, 79, 9, and 5 mM) in the bath (Fig. 6 A). Tonicity at low salt concentrations was maintained by the addition of mannitol. When the reversal potentials for nine experiments were plotted as a function of the log sodium activity (Fig. 6 B), the line predicted by the Nernst equation was within the standard deviations of the data although the data fall somewhat above the line. This deviation cannot be explained by a chloride permeability, but the deviation may be explained if sodium does not fully dissociate from the HEPES, EGTA, EDTA, or cGMP as assumed or if the molar ratio of Na to cGMP was lower than stated by the supplier.

Similar results were obtained with potassium (Fig. 6, C and D) and lithium (data not shown). In the case of potassium, the data lie much closer to the prediction of the Nernst equation. There was also less deviation at low concentrations. If the channel were permeable to chloride, the relation between ion concentration and reversal potential would show a departure from linearity at low concentrations similar to that observed here. If one were to assume that the deviation of the reversal potential from the Nernst potential in KCl is due entirely to chloride permeability, then the permeability ratio P_{Cl}/P_{Na} as determined by the GHK equation (Fig. 6 D, *dashed line*) must be <0.01 . This value is threefold lower than the upper limit of the chloride permeability in the rod channel estimated by Zimmerman and Baylor (1992) and is in agreement with the conclusions of Picones and Korenbrot (1992) in the bass cone and Menini (1990) in salamander rod that the cGMP-gated channels are very selective for cations over chloride.

Concentration Dependence of the Conductance

The current-voltage relations in Fig. 6, A and C, show that there is only a $\sim 50\%$ decrease in the conductance of the channel as the concentration of permeant ions is reduced from 500 to 5 mM. To show this more clearly, the chord conductance at $+80$ mV was plotted for each concentration of Na (Fig. 7 A, $n = 8$) and K (Fig. 7 B, $n = 6$). Because each patch represented in this plot contained a different number of channels, the conductances were normalized to the conductance obtained from a given patch at 100 mM. For both Na and K, the concentration ranged from 10 to 500 mM (see above for activities). The K activity giving half the maximum conductance was ~ 5 mM; the Na activity, between 5 and 10 mM. The later value was confirmed by analysis of the amplitudes of individual channel openings like those shown in Fig. 7 D (12 patches, 37 determinations). These traces were obtained in symmetrical sodium solutions with concentrations ranging from 20 to 500 mM at $+50$ mV. Fig. 7 C is a plot of the conductances obtained from such experiments and also includes nine points from the data of Haynes and Yau (1990) which were obtained from channels in symmetrical 120 mM sodium solutions. Under these conditions, the Na activity at which the conductance was reduced by half was <20 mM. Under symmetric ionic conditions, the concentration dependence of conductance should be described by a Michaelis relation (Läuger, 1973). Fitting such a relation to the data yields an estimated dissociation constant of 14 mM at $+50$ mV. A similar value was obtained at -50 , and somewhat lower (6 mM) at ± 30 mV. These values are in good agreement with those obtained in frog rods by Furman and

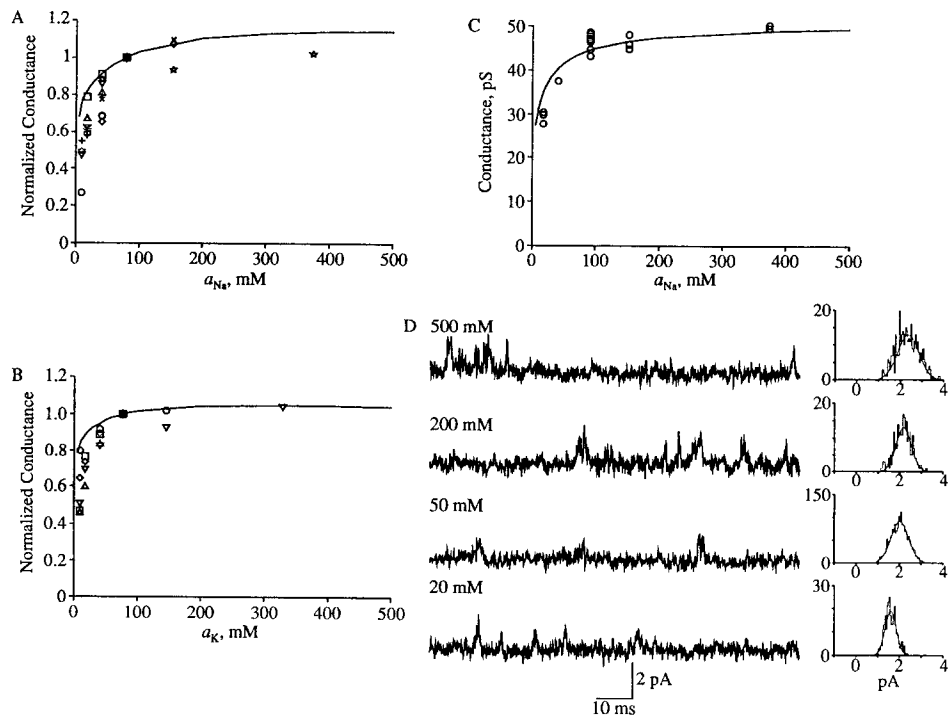


FIGURE 7. Concentration dependence of the conductance. The chord conductance at +80 mV is plotted as a function of sodium (A) or potassium (B) activity on the cytoplasmic side of the patch, normalized to the chord conductance at 100 mM. Each symbol represents a different experiment (eight for sodium, six for potassium). The curves are those predicted by the single-site Eyring rate theory model shown in Fig. 8 (parameters in Table II). (C) The unit conductance was obtained from analysis of individual channel openings at +50 mV in symmetric sodium solutions and is plotted as a function of the sodium activity. (D) Single-channel traces obtained in symmetric sodium solutions of 500, 200, 50, and 20 mM (activities of 374, 152, 79, 41, 17 mM). All of the patches were clamped at +30 mV and are plotted here with a bandwidth of 2.5 kHz. All traces are from different patches. The inset with each trace shows the open-amplitude histogram obtained from analysis of the full stretch of data from which the sample was excerpted. Each histogram is fitted with a single gaussian curve with a mean \pm SD for 500, 200, 50, and 20 mM Na (respectively) of 2.36 ± 0.49 , 2.18 ± 0.35 , 2.01 ± 0.41 , and 1.59 ± 0.26 pA.

Tanaka (1990), but are somewhat lower than those generally obtained for sodium (Naranjo and Latorre, 1993) and potassium channels (e.g., Latorre and Miller, 1983).

Such low values for the dissociation constant might suggest that there is a surface charge near the mouth of the pore which keeps the local concentration of ion high as the total concentration and ionic strength are lowered. If this were the case, then the conductance of the channel should be higher at low ionic strength than predicted by a simple Michaelis relation (Bell and Miller, 1984). Such a deviation is not apparent in the data, but data well below the dissociation constant could not be

obtained. If this deviation is truly absent, this would suggest that surface charge may not play an important role and that the channel has a somewhat higher affinity for cations than sodium and potassium channels generally.

DISCUSSION

These results show that the cGMP-gated channels of catfish cone outer segments are nonselective cation channels with little capacity to discriminate between lithium, sodium, potassium, and rubidium. Only ammonium and cesium show markedly different permeabilities relative to sodium. Under symmetrical conditions, it is clear that the conductance is greatest for NH_4 , followed by Na, K, Rb, and Cs. The permeability sequence of the cone channel fails to exactly match any of the classical Eisenman sequences (reviewed in Eisenman and Horn, 1983), but is closest to the "strong field" sequence IX albeit with an anomalously low sodium permeability. A high field strength model is also consistent with the apparently perfect exclusion of anions.

Is the Channel a Multi-Ion Pore?

Multiple occupancy of the channel would be demonstrated by concentration-dependent permeability ratios, anomalous mole fraction behavior, conductance-concentration relations with multiple dissociation constants or blockers with values for δ (the fraction of the membrane voltage crossed by a charged blocker to reach its binding site) exceeding 1. Of these tests, only the anomalous mole fraction behaviour was tested in detail here. Reducing the concentration of ions to the very low levels required to conclusively fail to observe concentration dependence in either the permeability or conductance ratios or multiple dissociation constants was not pursued here because of the lack of inert ions to maintain constant surface potential. All of the ions tested (choline, tetramethyl-, tetraethyl- and tetrapropylammonium, *N*-methyl-D-glucamine and Tris) also partially blocked the channel from the cytoplasmic side (Stotz and Haynes, 1995). Initial attempts using a concentration of 60 mM failed to show such a concentration dependence (data not shown), possibly because the channel is still effectively saturated, as demonstrated by the concentration-dependence of the conductance with sodium or potassium (Fig. 7). In contrast, Furman and Tanaka (1990) found that the permeability ratios obtained from the cGMP-gated channel of frog rods changed when the concentration of the ions was reduced (symmetrically) from 120 to 20 mM. It is difficult to explain why concentration-dependent permeability ratios should be found in one case but not the other since the 20 mM solutions used by Furman and Tanaka were also well above saturation of the conductance-concentration relation as determined by them ($K_D < 10$ mM). In the present study, there was also no sign of multiple dissociation constants over the very limited range of concentrations tested.

Multiple occupancy was explicitly tested by examining the sodium-lithium mole fraction behavior of the channel. Anomalous mole fraction behavior was not observed when substituting lithium for sodium, but the lack of anomalous mole fraction behavior does not necessarily exclude multiple occupancy, as has been demonstrated in dihydropyridine-sensitive calcium channels (Yue and Marban, 1990). It

must be concluded that the failure of these experiments to show multiple occupancy of the cone channel do not rule out a multi-ion channel, but neither do they provide any support for multiple occupancy of the channel by monovalent cations.

Eyring Rate Theory Models

One way in which to tie together the observations from the experiments presented here is to build a model of the permeation process. Eyring rate theory, as applied to channels, views the permeation of an ion as a process in which ions hop over energetically unfavorable barriers and bind in energetically favorable wells. The heights of these barriers and the depths of these wells vary with the type of ion, but their position across the electric field and their number remains fixed for a given model. While this view is certainly oversimplified, it does have the virtue of being computationally tractable.

Three Eyring models were fitted to the data. The first was a one-site, two-barrier model; the second, a two-site, three-barrier, single-occupancy model; the third, a two-site, three-barrier, double-occupancy model. The values for the positions and magnitudes of the energy barriers and wells and values for the surface charge were derived by fitting each of the models to a large data set derived by taking samples at 10-mV increments from the current-voltage relations from the biionic experiments (e.g., Fig. 1 and 2), the single-channel measurements (e.g., Fig. 3 and 4) and the concentration dependence of the single-channel conductance in sodium (e.g., Fig. 7 B), a total of 1,907 data points. The currents from multichannel patches were normalized using Eq. 2 to have the same magnitude as the current through a single channel. When fitting these models, all six ions were fitted simultaneously and all of the parameters listed above were allowed to vary. The slight outward rectification of the open-channel current indicates that a location for the binding site (for the two barrier, one binding site models) somewhat <50% of the way across the voltage drop should be expected for a channel whose binding site is flanked by barriers of the same height, and this was used as the initial position before obtaining a fit.

In general, the data from experiments using monovalent cations could be adequately fitted by simple one-site, two-barrier models. More complicated models did

TABLE II
Parameters for a Two-Barrier, Single-Site Eyring Model

Ion	Peak 1	Well	Peak 2
Li	6.28	-8.39	5.07
Na	6.43	-7.23	4.94
K	6.19	-7.18	5.14
Rb	6.47	-7.79	4.93
Cs	6.50	-8.05	5.63
NH ₄	5.45	-8.11	4.05
Distance	0.46	0.76	0.96

Surface charge (cytoplasmic side): 0.0322 C m⁻². Surface charge (extracellular side): 0.0038 C m⁻². Energies in units of kT; distance is in fraction of the electric field drop (0 at cytoplasmic side). The conventions and standard state used here are those described by Alvarez et al. (1992).

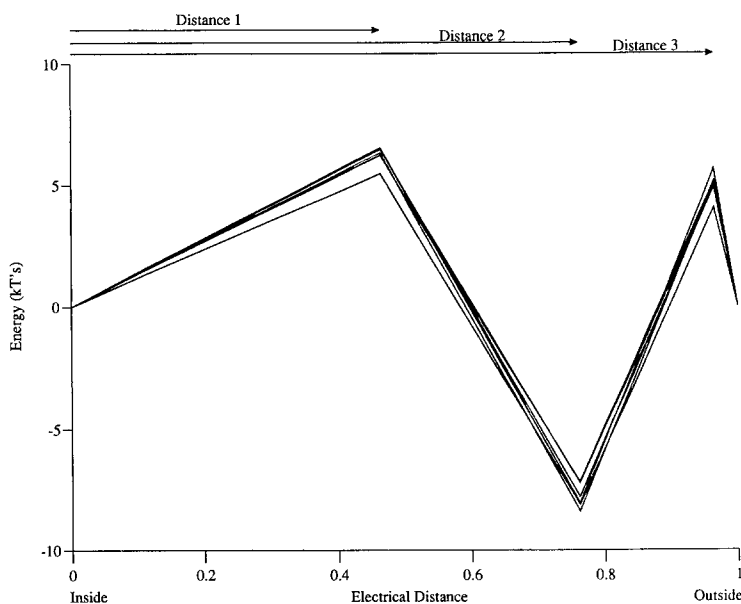


FIGURE 8. Schematic diagram of a two-barrier single-site Eyring model. The energy of each peak and the ion binding site are given in values of kT . The position of each peak or binding site is plotted as the fraction of the electric field drop crossed by an ion moving from the cytoplasmic side (0) to the extracellular side (1) of the channel. See Table II for the exact values. Each line represents a different ion. The tight grouping of the lines reflects the similar behavior of the ions.

not improve the fit, even when multiple occupancy was allowed, and often degenerated into the one-site, two-barrier model. The parameters for this model are given in Table II and are plotted schematically in Fig. 8. The ability of the model to predict the observed currents successfully is shown in Fig. 9 and in the curves in Figs. 3 B, 5 B, 7, A–C.

In this model, the first peak was at 0.46, the well at 0.76, and the last barrier at 0.96. The internal surface charge was quite reasonable, 0.032 C m^{-2} (1 charge per 497 \AA^2), whereas the external surface charge was relatively low (0.004 C m^{-2} , or 1 charge per $4,239 \text{ \AA}^2$). These values would argue that the energy values for the barriers and the wells are likely to be accurate since they are unbiased by the surface charge. The locations of the barriers and the well across the electric field drop are not very different from those of Picones and Korenbrot (1992), although it is difficult to make the comparison because they used different values for each ion. The values for the energies of the barriers and the well that they obtained are quite different because they were unable to scale their data by the number of channels in the patch and so were forced to use an arbitrary scaling factor. The model presented here, on the other hand, does a good job of predicting the single-channel currents observed under symmetrical ionic conditions (Figs. 3 B, 7 C, and 9) and the currents obtained under biionic conditions (Fig. 9). For Li, Na, K, Rb and Cs, the current predicted by the model closely approximates the observed current; the

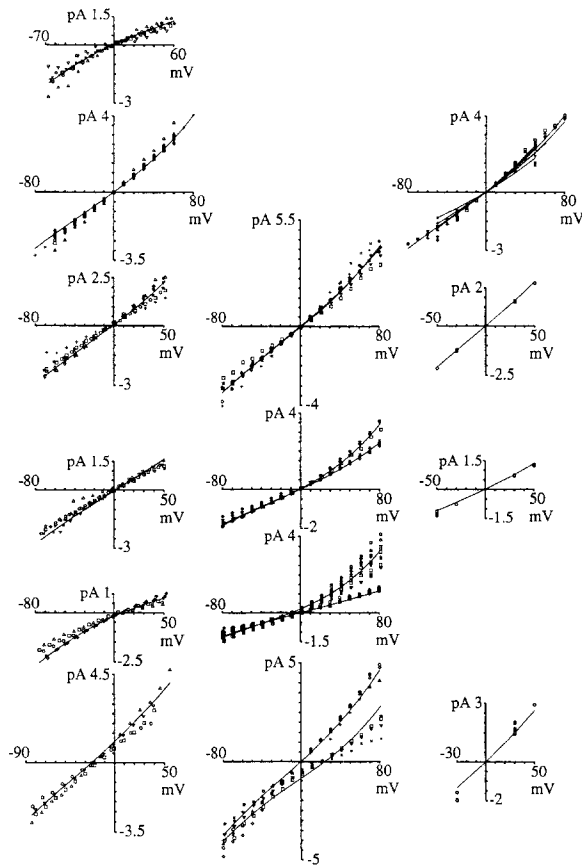


FIGURE 9. Current-voltage relations predicted by the model. From left to right, each column of current-voltage relations is for biionic experiments with external Na, biionic experiments with internal Na and single-channel measurements under symmetrical conditions. Each row represents a different test ion; Li, Na, K, Rb, Cs, and NH_4 from top to bottom. The various symbols represent data points from experiments while the solid line is the current predicted by the model. The single-channel current-voltage relation for Na contains data at 20, 50, 120, 200, and 500 mM whereas the others contain data at only 120 mM. No single-channel current-voltage relation is shown for Cs because data were obtained at only one voltage.

fit is less good for external NH_4 vs internal Na. Nonetheless, the simple two-barrier, one-site model it is remarkably good at predicting the observed currents carried by monovalent cations. As I will show in the next paper (Haynes, 1995), a very similar model also deals well with divalent cations.

Rectification of the Current-Voltage Relation

Unexpectedly, the single-channel current-voltage relation displayed outward rectification (see Fig. 4). Furthermore, the macroscopic current-voltage relations can be scaled to match the single-channel current-voltage relations using Eq. 2 (see Methods) without a voltage-dependent open probability term. This suggests that, in the presence of a saturating concentration of cGMP, there is no voltage dependence in the closed-open transition and that all of the rectification in the macroscopic current-voltage relation is due to the permeation process.

Haynes and Yau (1990) observed voltage dependence in the half-saturating concentration of cGMP and explained this on the basis of a voltage-dependent open probability. If this voltage dependence does not exist, then another explanation must be sought. Such a decrease in the half-saturating concentration of cGMP

upon depolarization could come about if the binding of cGMP were voltage dependent. For two reasons, it is unlikely that this voltage dependence could arise from the cGMP molecule crossing a portion of the electric field before reaching its binding site. First, the charge of the molecule is negative and a negatively charged molecule should bind less tightly upon depolarization rather than more tightly. Second, the structure of the rod and cone cGMP-gated channels (Bönigk, Altenhofen, Müller, Dose, Illing, Molday, and Kaupp, 1993) is such that the binding site is outside of the membrane proper, making it unlikely that it would directly experience the transmembrane electric field. It is nonetheless possible that the transmembrane voltage can favor certain conformations of the protein which distort the shape of the cGMP binding site. This would lead to voltage-dependent changes in either the association or dissociation rates for cGMP from the site. An independent piece of evidence in favor of this argument for voltage-dependent conformational changes in the channel structure is the voltage-dependent block of the channel by diltiazem (Haynes, 1992). The block occurs regardless of the charge of the diltiazem molecule and so the voltage dependence in the block is intrinsic to the channel protein, rather than the blocker. Thus, while the overall gating of the channel is voltage independent, one can imagine that certain conformational changes required for channel opening are, in fact, voltage dependent and that these conformations alter the shape of the cGMP binding pocket.

I wish to thank Maria J. Polyak for technical assistance. Thanks also to Drs. S. A. Barnes, R. J. French, and K. Hoehn for helpful discussion and critical reading of the manuscript.

This work was supported by the Alberta Heritage Foundation for Medical Research and the Medical Research Council of Canada.

Original version received 30 August 1994 and accepted version received 14 April 1995.

REFERENCES

- Alvarez, O., A. Villarroel, and G. Eisenman. 1992. Calculation of ion currents from energy profiles and energy profiles from ion currents in multibarrier, multisite, multioccupancy channel model. *In Methods in Enzymology*. Vol. 207. Ion Channels. B. Rudy and L. E. Iverson, editors. Academic Press, Inc., San Diego, CA. 816–854.
- Barry, P. H., and J. W. Lynch. 1991. Liquid junction potentials and small cell effects in patch-clamp analysis. *Journal of Membrane Biology*. 121:101–117.
- Bell, J. E., and C. Miller. 1984. Effects of phospholipid surface charge on ion conduction in the K⁺ channel of sarcoplasmic reticulum. *Biophysical Journal*. 45:279–287.
- Bönigk, W., W. Altenhofen, F. Müller, A. Dose, M. Illing, R. S. Molday, and U. B. Kaupp. 1993. Rod and cone photoreceptor cells express distinct genes for cGMP-gated channels. *Neuron*. 10:865–877.
- Colamartino, G., A. Menini, and V. Torre. 1991. Blockage and permeation of divalent cations through the cyclic GMP-activated channel from tiger salamander rods. *Journal of Physiology*. 440: 189–206.
- Colquhoun, D., and F. J. Sigworth. 1983. Fitting and statistical analysis of single-channel records. *In Single-Channel Recording*. B. Sakmann and E. Neher, editors. Plenum Publishing Corp., NY. 191–263.
- Eisenman, G., and R. Horn. 1983. Ionic selectivity revisited: the role of kinetic and equilibrium processes in ion permeation through channels. *Journal of Membrane Biology*. 76:197–225.

- Fesenko, E. E., S. S. Kolesnikov, and A. L. Lyubarsky. 1985. Induction by cyclic GMP of cationic conductance in plasma membrane of retinal rod outer segment. *Nature*. 313:310–313.
- Furman, R. E., and J. C. Tanaka. 1990. Monovalent selectivity of the cyclic guanosine monophosphate-activated ion channel. *Journal of General Physiology*. 96:57–82.
- Grahame, D. C. 1947. The electrical double layer and the theory of electrocapillarity. *Chemical Reviews*. 41:441–501.
- Haynes, L. W. 1991. Mono- and divalent inorganic cation selectivity of the cGMP-gated channel of catfish cone outer segments. *Journal of General Physiology*. 98:13a. (Abstr.)
- Haynes, L. W. 1992. Block of the cyclic GMP-gated channel of vertebrate rod and cone photoreceptors by *L-cis*-diltiazem. *Journal of General Physiology*. 100:783–801.
- Haynes, L. W. 1993. Mono- and divalent cation selectivity of catfish cone outer segment cGMP-gated channels. *Biophysical Journal*. 64:A133. (Abstr.)
- Haynes, L. W. 1994. Asymmetry of the permeation pathway in catfish cone cGMP-gated channels. *Biophysical Journal*. 66:A355. (Abstr.)
- Haynes, L. W. 1995. Permeation and block by internal and external divalent cations of the catfish cone photoreceptor cGMP-gated channel. *Journal of General Physiology*. 106:507–523.
- Haynes, L. W., and K.-W. Yau. 1985. Cyclic GMP-sensitive conductance in outer segment membrane of catfish cones. *Nature*. 317:61–64.
- Haynes, L. W., and K.-W. Yau. 1990. Single-channel measurement from the cyclic GMP-activated conductance of catfish retinal cones. *Journal of Physiology*. 429:451–481.
- Hille, B. 1992. *Ionic Channels of Excitable Membranes*, Second Edition. Sinauer Associates, Inc., Sunderland, MA. 607 pp.
- Karpen, J. W., A. L. Zimmerman, L. Stryer, and D. A. Baylor. 1988a. Gating kinetics of the cyclic-GMP-activated channel of retinal rods: flash photolysis and voltage-jump studies. *Proceedings of the National Academy of Sciences, USA*. 85:1287–1291.
- Karpen, J. W., A. L. Zimmerman, L. Stryer, and D. A. Baylor. 1988b. Molecular mechanics of the cyclic-GMP-activated channel of retinal rods. *Cold Spring Harbor Symposia on Quantitative Biology*. Vol. LIII: 325–332.
- Läuger, P. 1973. Ion transport through pores: a rate-theory analysis. *Biochimica et Biophysica Acta*. 311: 423–441.
- Latorre, R., and C. Miller. 1983. Conduction and selectivity in potassium channels. *Journal of Membrane Biology*. 71:11–30.
- Menini, A. 1990. Currents carried by monovalent cations through cyclic GMP-activated channels in excised patches from salamander rods. *Journal of Physiology*. 424:167–185.
- Naranjo, D., and R. Latorre. 1993. Ion conduction in substates of the batrachotoxin-modified Na⁺ channel from toad skeletal muscle. *Biophysical Journal*. 64:1038–1050.
- Neher, E. 1992. Correction for liquid junction potentials in patch clamp experiments. In *Methods in Enzymology*, Vol. 207. Ion Channels. B. Rudy and L. E. Iverson, editors. Academic Press, Inc., San Diego, CA. 123–131.
- Picones, A., and J. L. Korenbrot. 1992. Permeation and interaction of monovalent cations with the cGMP-gated channel of cone photoreceptors. *Journal of General Physiology*. 100:647–673.
- Picones, A., and J. L. Korenbrot. 1994. Analysis of fluctuations in the cGMP-dependent currents of cone photoreceptor outer segments. *Biophysical Journal*. 66:360–365.
- Pitzer, K. S., and G. Mayorga. 1973. Thermodynamics of electrolytes. II. Activity and osmotic coefficients for strong electrolytes with one or both ions univalent. *Journal of Physical Chemistry*. 77:2300–2308.
- Robinson, R. A., and R. H. Stokes. 1970. *Electrolyte Solutions. The Measurement and Interpretation of Conductance, Chemical Potential and Diffusion in Solutions of Simple Electrolytes*. Second edi-

- tion (revised). Butterworths and Co., Ltd., London. 31–32.
- Stotz, S. C., and L. W. Haynes. 1995. Block of cone cGMP-gated channels by internal organic cations. *Biophysical Journal*. 68:A386. (Abstr.)
- Torre, V., M. Straforini, F. Sesti, and T. D. Lamb. 1992. Different channel-gating properties of two classes of cyclic GMP-activated channel in vertebrate photoreceptors. *Proceedings of the Royal Society of London, B*. 250:209–215.
- Yau, K.-W. and L. W. Haynes. 1986. Effect of divalent cations on the macroscopic cGMP-activated current in excised rod membrane patches. *Biophysical Journal*. 49:33a. (Abstr.)
- Yau, K.-W., L. W. Haynes, and K. Nakatani. 1986. Roles of calcium and cyclic GMP in visual transduction. In *Control of Cellular Activity*. H. Ch. Lüttgau, editor. F. Fischer, Stuttgart, and Sinaur Associates, Inc., Sunderland, MA. 343–366.
- Yue, D. T., and E. Marban. 1990. Permeation in the dihydropyridine-sensitive calcium channel. Multion occupancy but no anomalous mole-fraction effect between Ba^{2+} and Ca^{2+} . *Journal of General Physiology*. 95:911–939.
- Zimmerman, A., and D. A. Baylor. 1986. Cyclic GMP-sensitive conductance of retinal rods consists of aqueous pores. *Nature*. 321:70–72.
- Zimmerman, A., and D. A. Baylor. 1992. Cation interactions within the cyclic GMP-activated channel of retinal rods from the tiger salamander. *Journal of Physiology*. 449:759–783.